Research paper

Effect of the treatment with H_3PO_4 on the catalytic activity of Nb_2O_5 supported on Zr-doped mesoporous silica catalyst. Case study: Glycerol dehydration

C. García-Sancho[a], J.A. Cecilia[b], J.M. Mérida-Robles[b], J. Santamaría González[b], R. Moreno-Tost[b,*], A. Infantes-Molina[b], P. Maireles-Torres[b]

[a] Grupo de Energía y Química Sostenibles (EQS), Instituto de Catálisis y Petroleoquímica (CSIC) C/Marie Curie 2, 28049 Madrid, Spain
[b] Universidad de Málaga, Departamento de Química Inorgánica, Cristalografía y Mineralogía (Unidad Asociada al ICP-CSIC), Facultad de Ciencias, Campus de Teatinos, 29071 Málaga, Spain

ARTICLE INFO

ABSTRACT

We have previously demonstrated the influence of the niobium species over the glycerol dehydration reaction and how the catalyst regeneration by thermal treatment modified the catalytic performance due to the transformation of superficial niobium species. This experimental conclusion encouraged us to find a way to maintain and even improve the catalytic behavior of these Nb-based catalysts. Thus, herein, it is reported the influence of phosphoric acid treatment on 8 wt% Nb_2O_5 supported on a zirconium doped mesoporous silica (Si/Zr = 5 molar ratio) catalyst, varying the Nb/P molar ratio between 0.1 and 1. Catalysts were full characterized and tested in the glycerol dehydration at 325 °C. This acid treatment modifies the nature of species present on the catalyst surface, as inferred from ^{31}P NMR data, where the presence of zirconium hydrogenphosphate was detected. A comprehensive study of the influence of acid properties on the catalytic activity has been carried out. Thus, the selectivity to acrolein was improved, which was attributed to this hydrogenphosphate phase and the catalyst stability was associated to the existence of acid sites of low and moderate strength. The best catalyst was studied at higher reaction temperatures, showing the highest glycerol conversion and achieving an acrolein selectivity of 74%, at 350 °C. This catalyst was also regenerated, maintaining its catalytic activity.

1. Introduction

In the last years, the development of new catalytic processes for the production of fuels and chemicals from renewable feedstock has been greatly encouraged due to the depletion of fossil resources and environmental concerns. In this context, biodiesel is considered as a promising alternative fuel, with a lower environmental impact than conventional fuels. It is mainly produced from transesterification of vegetable oils and animal fats with short-chain alcohols, mainly methanol and ethanol, obtaining glycerol as by-product [1–3]. Thus, about 1 kg glycerol is roughly obtained per each 10 kg of biodiesel, so that large amounts of glycerol surpluses are generated, causing a drop in its price [4,5]. Therefore, glycerol has become an interesting feedstock for the synthesis of high value-added products, which in some cases are currently produced in the petrochemical industry from oil. Thus, new uses of glycerol are being researched to attain a sustainable biodiesel production.

One of the most promising routes for glycerol valorization lies in its catalytic dehydration to acrolein, which is an important intermediate for the chemical industry and it is employed for the synthesis of acrylic acid and its esters, D,L-methionine, glutaraldehyde, polyurethanes and polyester resins [6]. Although industrial acrolein production is based on partial oxidation of propylene, coming from fossil fuels, catalyzed by multicomponent $BiMoO_x$ based catalysts, there is a growing interest to transform acrolein into glycerol [6,7]. The catalytic conversion of glycerol to acrolein, by a double–dehydration reaction, is an acid-catalyzed process. In this sense, several solid acid catalysts have been proposed for the gas-phase selective conversion of glycerol into acrolein, including heteropolyacids [8–12], zeolites [13–16], metal and mixed oxides [17–20], phosphates and pyrophosphates [21–24], sulfated zirconia [25,26] and sulfonic-functionalized SBA-15 [27]. Different authors have confirmed that the catalytic activity depends strongly on the textural, mainly the pore size, and acid properties of solid catalysts [7,28].

It has been recognized in the literature that niobium oxide exhibits excellent acid properties and hydrothermal stability [29,30]. Chai et al.

[31] showed that niobium oxide is an effective catalyst for the gas-phase dehydration of glycerol and studied the influence of calcination temperature. Likewise, different mixed metal oxides, containing niobium, have been tested for this reaction, such as $WNbO_x$ [32] and $ZrNbO_x$ [33,34]. As niobium oxide possesses a low specific area, high-surface area supports are often employed to enhance the dispersion of active phases and increase the number of available active sites. Thus, Shiju et al. [19] prepared a series of silica-supported niobia catalysts for the dehydration of glycerol to acrolein. They stated that the catalytic performance was strongly influenced by the total acidity, which depended on the niobia loading and calcination temperature. Moreover, niobium and tungsten mixed oxides have been evaluated over different supports, such as ZrO_2, Al_2O_3, SiO_2 and TiO_2 [4,35], obtaining high acrolein yields in presence of these catalysts.

On the other hand, the type of acid sites is a key parameter influencing the catalytic performance. It is generally accepted that Brönsted acid sites are more selective to acrolein than Lewis acid sites [15,36–38]. In addition, Lauriol-Garbay et al. [33] confirmed that a reduction of the number of Lewis acid sites improved the stability of catalysts. Moreover, it is known that niobium oxide possesses both Lewis and Brönsted acid sites when is supported on silica [30,39,40]. Furthermore, several authors have demonstrated that when Nb_2O_5 is treated with phosphoric acid, the total acidity and strength of acid sites are enhanced [41–44]. Hence, Lee et al. [45] evaluated the incorporation of different amounts of phosphate to Nb_2O_5, in such a way that this treatment ameliorated its acidic properties. In this sense, the greater the phosphate loading, the higher the amount of acid sites detected on the catalyst surface, improving consequently the glycerol conversion and acrolein selectivity. Likewise, a mesoporous siliconobium phosphate, prepared by Choi et al. [46], was employed as Brönsted acid catalyst for glycerol dehydration to acrolein. This material displayed high activity and stability attributed to the nearly pure Brönsted acidity, which promoted the formation of acrolein, and large mesopores which significantly reduced pore blocking by coke deposition. Therefore, the use of mesoporous materials favors the dispersion of the active phase and hinders the deactivation processes. Moreover, the incorporation of heteroatoms, such as Al, Zr or Ti, in the synthesis step of mesoporous silica can generate a higher number of acid centers [47]. Katryniok et al. also corroborated that the doping with zirconium enhances the acidity of the support and the catalyst stability [48].

In a previous study, it was found that niobium incorporation to a zirconium doped mesoporous silica had a noticeable influence on the nature of superficial niobium species, and consequently on the catalytic performance in glycerol dehydration [49]. Those results encourage us to improve the catalytic performance of the best catalyst assayed. Thus, a niobium catalyst supported on a Zr-doped SBA-15 silica with a loading of 8 wt% Nb_2O_5 was undergone to a treatment with phosphoric acid, synthesizing a family of catalysts with different Nb/P molar ratio. The main goal of this work was to evaluate the influence of such treatment on both textural and acid properties, and how the variation of these properties affects the catalytic activity and special attention was paid to the reusability and deactivation of catalysts.

2. Experimental

2.1. Preparation of catalysts

The preparation details of the support (labeled as *Zr*) and the catalyst with a 8 wt% of Nb_2O_5 (*ZrNb*) have been previously reported [49]. Thus, ZrNb was prepared by means of incipient wetness impregnation with a niobium oxalate solution to achieve 8 wt% Nb_2O_5 and subsequent calcination at 400 °C for 4 h. The *ZrNb* catalyst was treated with aqueous solutions of H_3PO_4 to attain different Nb/P molar ratio by using also the incipient wetness impregnation method. Next, these materials (denoted as *ZrNbPx*, where *x* indicated the Nb/P molar ratio employed; *x* = 0.1-1) were dried at 60 °C, calcined at 400 °C for 4 h.

Another catalyst with a Nb/P molar ratio of 0.2 was prepared by impregnation of the *Zr* support with a niobium oxalate − oxalic acid solution (8 wt% Nb_2O_5), and after drying at 60 °C overnight, it was impregnated with a phosphoric acid aqueous solution (Nb/P molar ratio of 0.2), dried at 60 °C and calcined at 400 °C. This latter catalyst was subjected to just one calcination procedure; therefore, to distinguish it from the ZrNbPx catalyst, it was named as *ZrNbP0.2-1c*, where *1c* emphasizes that one calcination step was carried out.

For comparison reasons, a catalyst without niobium (*ZrP0.2*) was prepared following the same recipe as the *ZrNbP0.2* catalyst, excepting the addition of the niobium precursor. Likewise, a SBA-15 silica without zirconium was synthesized and used as support to prepare a catalyst (*NbP0.2-1c*) following the same procedure as for *ZrNbP0.2-1c*.

A list of the synthesized catalyst can be found in the Supplementary Information.

2.2. Characterization of catalysts

Powder X-ray diffraction patterns were collected on an X́Pert Pro MPD automated diffractometer (PANanalytical) equipped with a Ge (1 1 1) primary monochromator (strictly monochromatic Cu-Kα radiation) and a X'Celerator detector.

The textural parameters were determined from the nitrogen adsorption–desorption isotherms at −196 °C, obtained by using an automatic ASAP 2020 model of gas adsorption analyser from Micromeritics. Prior to N_2 adsorption, the samples were outgassed at 200 °C and 10^{-4} mbar for 10 h. Surface areas were determined by using the Brunauer–Emmett–Teller (BET) equation and a nitrogen molecule cross section of 16.2 $Å^2$. The Density Functional Theory method (DFT) was employed to determine the pore size distribution.

X-ray photoelectron spectra were obtained with a Physical Electronics PHI 5700 spectrometer with non-monochromatic Mg Kα radiation (300 W, 15 kV, and 1253.6 eV) with a multi-channel detector. Spectra were recorded in the constant pass energy mode at 29.35 eV, using a 720 μm diameter analysis area. Charge referencing was measured against adventitious carbon (C 1s at 284.8 eV). A PHI ACCESS ESCA-V6.0 F software package was used for acquisition and data analysis. A Shirley-type background was subtracted from the signals. Recorded spectra were always fitted using Gaussian–Lorentzian curves in order to determine the binding energies of the different element core levels more accurately.

FTIR spectra were collected on a Varian 3100 FT-IR spectrophotometer, and the samples were diluted in KBr.

The temperature-programmed desorption of ammonia (NH_3-TPD) was carried out to evaluate the total surface acidity. The catalyst (80 mg) was treated by increasing the temperature from room temperature up to 400 °C with a heating rate of 10 °C min^{-1}, and maintained at 400 °C for 15 min under a helium flow. Right after, the catalyst was cooled at 100 °C, it was put in contact with an ammonia flow. The NH_3-TPD was performed by raising the temperature from 100 to 550 °C, under a helium flow of 40 mL min^{-1}, with a heating rate of 10 °C min^{-1}, and maintained at 550 °C for 15 min. The evolved ammonia was analyzed by using a TCD detector of a gas chromatograph (Shimadzu GC-14A).

FTIR spectra after pyridine adsorption were recorded on a Shimadzu Fourier Transform Infrared Instrument (FTIR8300). Self supported wafers of samples with a weight/surface ratio of about 15 mg cm^{-2} were placed in a vacuum cell greaseless stopcocks and CaF_2 windows. Samples were thermally treated at 300 °C and 10^{-4} mbar overnight, exposed to pyridine vapors at room temperature (pressure of 200 mbar) for 10 min, and then outgassed at 200 °C. The amount of both Brönsted and Lewis acid sites have been calculated from integrated areas of the bands located about 1450 (19b vibration mode) and 1550 cm^{-1} (19b vibration mode) using the extinction coefficients E_L = 1.11 cm $μmol^{-1}$ and E_B = 0.73 cm $μmol^{-1}$, respectively [50].

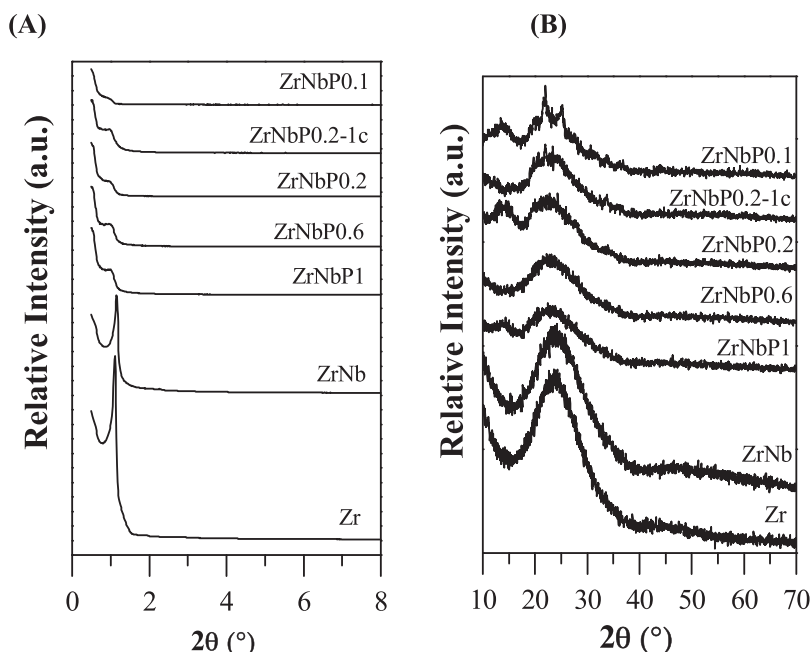Thermogravimetric analysis (TGA) of spent catalysts was carried out

(A)

(B)

with a TGA/DSC 1 model (Mettler-Toledo), measuring the weight variation in presence of air flow of 50 mL min^{-1} with a heating ramp of 10 °C min^{-1}, from room temperature until 900 °C. The carbon content of spent catalysts was measured with a LECO CHNS 932 analyser.

^{29}Si and ^{31}P MAS NMR spectra were recorded on a Bruker AVIII HD 600 NMR spectrometer (field strength of 14.1 T), using zirconia rotors at 15 kHz spinning rates. ^{29}Si spectra were registered by using a 2.5 mm triple-resonance DVT probe. The experiments were performed with ^{1}H decoupling (cw sequence) by applying a single pulse (π/2), an excitation pulse of 5 μs, 60 s relaxation delay and 10800 scans. The chemical shift was referenced to an external solution of tetramethylsilane (TMS). ^{31}P MAS NMR spectra were recorded in a HXY, Efree MAS probe of 3.2 mm. CP-MAS and Hpdec sequences were used to register ^{31}P spectra. The chemical shift was referenced with respect to ammonium dihydrogenphosphate at 0.9 ppm.

2.3. Catalytic tests

The dehydration of glycerol was performed, at atmospheric pressure, in a fixed-bed continuous-flow stainless steel reactor (9.1 mm in diameter, and 230 mm in length), operated in the down-flow mode. The reaction temperature was measured with an interior placed thermocouple in direct contact with the catalyst bed. For the activity tests, 0.5 g of catalyst (particle size 0.85–1.00 mm), diluted with SiC to 3 cm^3 volume, were used. Catalysts were pre-treated in situ at atmospheric pressure under a N$_2$ flow of 15 mL min^{-1}, at 325 °C for 30 min. A glycerol solution (10 wt.% in water) was supplied by means of a Gilson 307SC piston pump (model 10SC) at 0.1 mL min^{-1} feed rate in a N$_2$ flow (15 mL min^{-1}). The evolution of the catalytic performance was studied by collecting liquid samples after 2 h and 8 h of time on stream in a vial cooled in an ice trap. These vials were sealed and analyzed by means of gas chromatograph (Shimadzu GC-14B), equipped with a flame ionization detector and a capillary column (TRB-14). The TRB-14 capillary column was provided by Teknokroma. The characteristics of the column were: 60 m of length, the internal diameter was of 32 mm with a film thickness of 20 μm.

The glycerol conversion (mol%), the selectivity to the identified products and the yields obtained have been calculated as follows:

$$C\,(\%) = \frac{n_{Gly,in} - n_{Gly,out}}{n_{Gly,in}} \times 100$$

$$S_i\,(\%) = \frac{n_i}{n_{Gly,in} - n_{Gly,out}} \times \frac{z_i}{z_{Gly.}} \times 100$$

$$y_i\,(\%) = \frac{C \times S_i}{100}$$

where n_{in} and n_{out} represent the mol of glycerol at the inlet and outlet of the reactor. n_i is the molar concentration of the product i at the outlet of the reactor and z_i and z_{Gly} are the number of carbon atoms of the product i and glycerol, respectively. The carbon balance (mol%) was calculated by summing up the unreacted glycerol and the total quantities of detected and calibrated products.

The Turn Over Frequency (TOF) values have been calculated as function of the mmol of glycerol converted per acid site (determined from NH$_3$-TPD) and per second. The equation was:

$$TOF = \frac{F_{Gly} * C_{Gly}}{m_{cat} * \text{Acid site} * 60}$$

where F_{Gly} represents the flow of glycerol fed (mmol Gly/min), C_{Gly} is the glycerol conversion, m_{cat} represents the mass of catalyst (g) and Acid site represents the concentration of acid sites measured by means of NH$_3$-TPD per gram of catalyst and finally, 60 is a factor of conversion between minutes and seconds.

3. Results and discussion

3.1. Characterization of catalysts

The physico-chemical characterization of the *Zr* support and the *ZrNb* catalyst was reported in a previous work [49], although some of these characteristics will be included in the present work for helping to a better understanding of results. Regarding their X-ray diffraction analysis (Fig. 1A), both samples exhibit a diffraction signal in the low-angle region, which confirms the formation of the typical hexagonal SBA-15 mesostructure, but the absence of the diffraction peaks corresponding to the (110), (200) and (210) planes would point out a low long-range order [51]. The intensity of this peak is reduced after the phosphoric acid treatment, being more drastic for catalysts with the lowest Nb/P molar ratio, although the lattice parameter, a$_0$, is not affected (Table S1, Supporting information). Therefore, it can be concluded that the mesostructure is partially preserved, which agrees well with the findings of Wu et al. [52], who also observed an intensity

decrease of the diffraction peaks at low-angle region when a SBA-15 silica was treated with H_3PO_4, resulting in a less ordered structure. The XRD patterns in the high-angle region (Fig. 1B) evidence that these catalysts show mainly amorphous siliceous walls, and neither crystalline Nb_2O_5 nor ZrO_2 phases have been detected. Only in the case of the *ZrNbP0.1* catalyst, several broad and less defined diffraction peaks are observed (Fig. 1B), which could be ascribed to zirconium [53] and niobium [54] phosphates, but unequivocal assignation to a particular phase is quite difficult.

The partial destruction of the mesostructure could also be inferred from TEM analysis. For Nb/P molar ratios between 0.6 and 1, micrographs show the characteristic hexagonal arrangement of channels in the SBA-15 structure, but this is less visible when the phosphorus loading increases, arising new dense particles which could be ascribed to such crystalline phases mentioned above (Fig. S1).

^{31}P solid state MAS NMR spectroscopy provides useful information regarding the local environment of phosphorus atoms, and the ^{31}P HPDEC (high power decoupling) MAS (magic angle spinning) NMR spectra of the *ZrNbPx* catalysts along with commercial hydrogenphosphate of zirconium (*c-ZrP*), niobium phosphate (*c-NbP*), *NbP0.2-1c* catalyst and *ZrP0.2* are displayed in Fig. 2.

A)

^{31}P Hpdec MAS NMR

c-ZrP
ZrNbP0.1
ZrNbP0.2
ZrNbP0.2-1c
ZrNbP0.6
ZrNbP1

δ (ppm)

B)

c-NbP
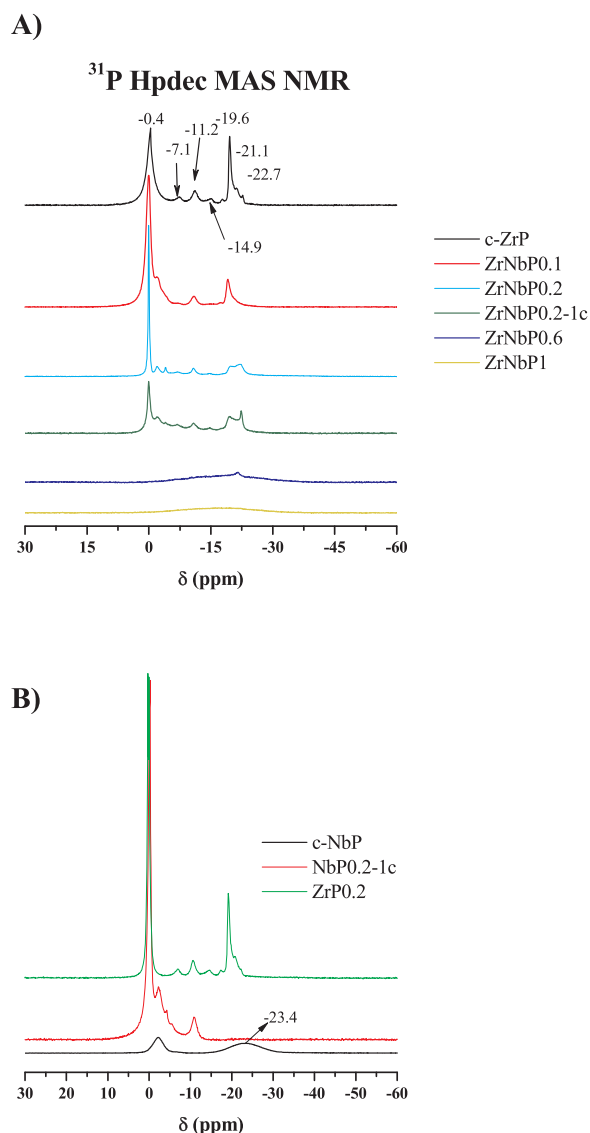NbP0.2-1c
ZrP0.2

δ (ppm)

Fig. 2. ^{31}P Hpdec MAS NMR spectra of the ZrNbPx catalysts and hydrogenphosphate of zirconium (c-ZrP) (A) and niobium phosphate (c-NbP), NbP0.2-1c and ZrP0.2 catalysts (B).

The *c-ZrP* solid shows an intense band at − 19.6 ppm together with other low intense ones at − 7.1, − 11.2, − 14.9, − 21.1 and − 22.7 ppm, and a broad and intense band at − 0.4 ppm (Fig. 2A). Hence, signals at − 7.1 ppm, at − 11.2 and − 14.9 ppm, and at − 19.6 and − 22.7 ppm can be ascribed to phosphorus atoms with one, two and three P–O–Zr bonds, respectively [55–58]. Thus, the − 19.6 ppm signal is associated to HPO_4^- groups, triply bonded to three zirconium atoms [58]. It is remarkable the absence of bands at higher chemical shift, which would reveal the presence of P–O–P bonds, typical of zirconium pyrophosphate [59–61]. Finally, the broad band at − 0.4 ppm is raised by free H_3PO_4 molecules [62–64]. The spectrum of *c-NbP* (Fig. 2B) displays a characteristic broad band at − 23.4 ppm [65].

On the other hand, the spectrum of *ZrP0.2* (catalyst without niobium in its composition) is identical to that of *c-ZrP*, and consequently zirconium hydrogenphosphate along with phosphoric acid are detected on the catalyst surface. Moreover, the narrow line at ca. 0.2 ppm is indicative of the high degree of mobility of phosphoric acid molecule [63]. However, the spectrum of the catalyst without zirconium (*NbP0.2-1c*) differs from those of commercial *ZrP* and *NbP*, and the bands can be attributed to phosphoric acid (ca. − 0.22 ppm) and phosphoric acid derived oligomers [63,64,66].

Concerning the spectra of *ZrNbPx* samples (Fig. 2A), as the phosphorus loading increases, the intensity of bands associated to the zirconium hydrogenphosphate is higher, although these are almost no detectable for *ZrNbP1*. On the other hand, the band at − 0.4 ppm is ascribed to H_3PO_4 occluded inside the pores of the catalyst [61]. Furthermore, the formation of a silicophosphate is ruled out because of the absence of upfield bands between − 30 and − 44 ppm [63]. To prove this assumption, the *ZrNbP0.2* catalyst was calcined at 700 °C, and its ^{29}Si NMR spectrum only exhibits bands associated to the siliceous network (Fig. S2), indicating that the reaction between phosphoric acid and silica does not take place [67]. Moreover, the intensity and narrowness of bands ascribed to zirconium hydrogenphosphate would confirm the high ordering degree, being more crystalline for *c-ZrP*. This result is in accordance with TEM analysis previously discussed, which showed the existence of particles without the characteristic hexagonal structure of SBA-15, and therefore, these particles could be ascribed to the formation of a zirconium phosphate phase. These results seem to prove that phosphoric acid has a stronger tendency to react with zirconium species and the crystalline phases observed in the XRD patterns were associated to zirconium hydrogenphosphate, thus causing the partial extraction of zirconium from the siliceous structure.

The $^1H \rightarrow ^{31}P$ cross polarization spectra (CP-MAS NMR) provides useful information about the presence or absence of protons in the neighboring of phosphorus atoms [64]. It is clearly shown that signals due to phosphoric acid and its condensed phases do not effectively cross polarize (Fig. 3), and these species are found in a liquid like environment [64]. Only samples containing zirconium hydrogenphosphate display cross polarization, being a proof of the existence of protons in POH groups. The *ZrNbP1* and *ZrNbP0.6* catalysts do not show any band, although this could be likely due to the amorphous character and low amount of zirconium phosphate species in these catalysts.

The textural properties have been evaluated from nitrogen adsorption-desorption isotherms at − 196 °C (Fig. S3), which are of type IV according to the IUPAC classification, even after the treatment with H_3PO_4, except for the catalyst with the lowest Nb/P molar ratio. This catalyst displays a typical isotherm of non-porous solids, with a large amount of nitrogen adsorbed at relative high pressures, due to interparticle porosity [68]. As expected, after supporting Nb_2O_5, both BET surface area and pore volume decrease (Table 1), and this effect is more pronounced after treatment with H_3PO_4. This evolution corroborates the partial collapse of the mesoporous structure with the amount of P species, in agreement with XRD and TEM data, as previously observed for V-P catalysts [69]. Ekhsan et al. also reported that the treatment of a niobium supported on TiO_2–SiO_2 with H_3PO_4 caused the destruction of the silica structure during the calcination [44]. Likewise, the textural

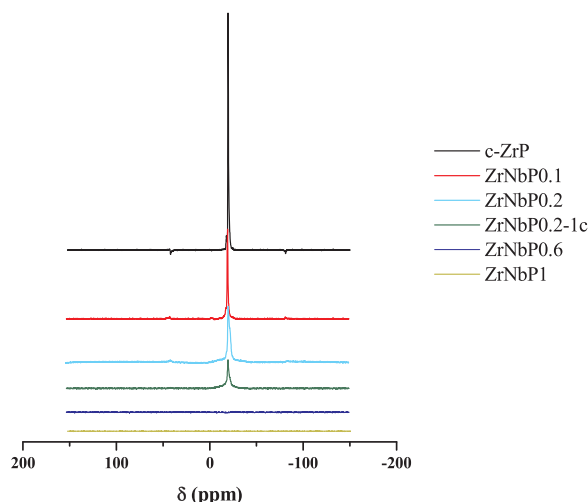Fig. 3. ^{1}H →^{31}P CP-MAS NMR spectra of the ZrNbPx catalysts.

Table 1
Textural and acidic properties of catalysts.

Sample	^{a}S$_{BET}$ (m^2 g^{-1})	V$_P$ (cm^3 g^{-1})	Pore size (nm)	^{b}μmoles NH$_3$ g$_{cat}$$^{-1}$	^{c}B/B + L
Zr	812	0.61	3.3	474 (0.58)	0.61
ZrNb	555	0.42	3.5	648 (1.17)	0.68
ZrNbP1	531 (137)	0.58 (0.20)	4.9 (6.5)	372 (0.70)	0.21
ZrNbP0.6	489 (134)	0.47 (0.19)	4.5 (6.3)	381 (0.78)	0.51
ZrNbP0.2	179 (75)	0.27 (0.20)	6.3 (11.9)	919 (5.13)	0.9
ZrNbP0.1	30 (16)	0.16 (0.10)	22.8 (29.9)	287 (9.57)	0.97
ZrNbP0.2-1c	316 (133)	0.39 (0.22)	4.8 (7.0)	1010 (3.19)	1.0
RZrNbP0.2-1c	190	0.36	6.5	804 (4.23)	0.96

^{a} In parentheses, textural parameters after catalytic test.
^{b} μmol NH$_3$/m^2 in parentheses.
^{c} Ratio of concentration of Brönsted respect total acid sites from the adsorption of pyridine evacuated at 200 °C.
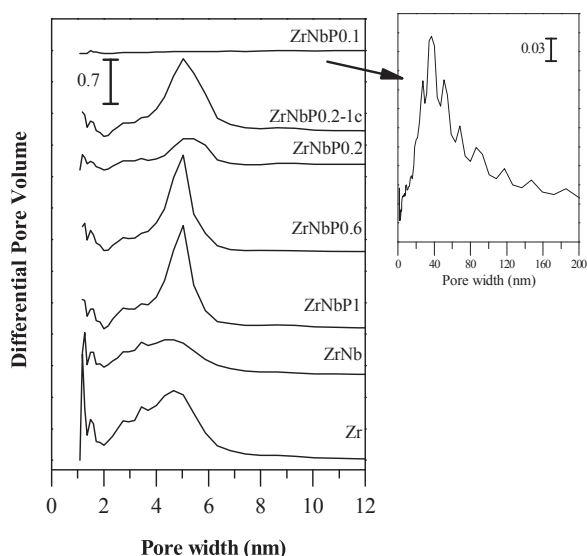

Fig. 4. Pore size distribution curves of ZrNbPx catalysts.

Table 2
Atomic ratio obtained by XPS results of fresh catalysts.

Sample	Atomic ratio	
	Zr/(Si + Nb) $_{XPS}$	Nb/(Si + Zr)$_{XPS}$
ZrNb	0.017	0.023
ZrNbP1	0.032	0.026
ZrNbP0.6	0.035	0.060
ZrNbP0.2	0.024	0.038
ZrNbP0.1	0.017	0.032
ZrNbP0.2-1c	0.033	0.041

values are within the range of mesopores (Table 1 and Fig. 4). The successive addition of elements to the support modifies the pore size distribution (Fig. 4). The addition of 8 wt% of Nb$_2$O$_5$ to the support causes that the distribution of pore sizes is not changed but the intensity of the peaks is lowered, due to the lower pore volume of the ZrNb catalyst. When the ZrNb catalyst is treated with phosphoric acid, a variation of the shape of the pore size distribution curve occurs. In this case, the smaller pores disappear and the pores centered over 5 nm are now stressed. The ZrNbP0.1 catalyst shows a wider distribution of pore sizes, from mesopores to macropores, in agreement with the textural parameters obtained.

XPS analysis has been used to characterize the surface composition of catalysts (Table 2 and Table S2). The incorporation of Zr(IV) into the siliceous framework is confirmed by a Zr 3$d_{5/2}$ signal at 183.2 eV, a binding energy (BE) value higher than that of pure ZrO$_2$ (182.2 eV) [70], which is attributed to Si-O-Zr bonds [47,71,72]. The BE value of Zr 3$d_{5/2}$ is hardly affected by the incorporation of niobium oxide (ca. 183 eV), but when the phosphorus loading is increased, a shift from 182.7 eV for the *ZrNbP1* catalyst up to 183.5 eV for *ZrNbP0.1* is found. This fact might indicate that phosphorus is located in the vicinity of Zr forming Zr–O–P bonds [61]. However, the BE for Zr 3$d_{5/2}$ band is approximately 2 eV lower than those reported for zirconium phosphate [59,70,73,74]. The observed shifts on the Zr 3d core level can reflect variations in the polarity of the Zr–O bond [70]. Indeed, the slight shift to higher binding energies would indicate a greater amount of hydroxyl groups on the surface of the *ZrNbP0.1* catalyst [59], thus increasing its acidity.

Regarding to O 1s region in *Zr* and *ZrNb* catalysts, an asymmetric and broad band, centered at ~532.8 eV and FWHM of ~2.3 eV, can be observed (Table 2), which can be decomposed into two contributions located at 530.7 and 533.0 eV. The most intense contribution at higher BE is characteristic of silica and the other band to Zr–O–Si bonds [75]. After treatment with phosphoric acid, the broader FWHM evidences the existence of oxygen in different environments, i.e., oxygen bonded to Zr, Si, Nb and P. Similarly to *Zr* and *ZrNb* solids, the O 1s signal can be decomposed into two components, at 531.5 eV and 533 eV, which are associated to oxygen bonded to Zr and Si, respectively (Table S2). On the other hand, the relative intensity of both bands is modified with the increment of the phosphorus loading, thus increasing the higher BE component in detriment of the band at 531.5 eV. This experimental evidence could lead us to think that there would be distinct oxygen species bonded to phosphorus, such as P-O-P, P = O or P-OH, as well as M-O-P where M could be Zr, Si or Nb, respectively. An oxygen doubled bonded to phosphorous, P = O species, will have a higher charge density [76,77] which would imply a contribution of this oxygen to the lower binding energy value. Likewise, the higher BE band could correspond to oxygen in P-O-P bonds [78], but these species were ruled out from NMR results, which discarded the existence of pyrophosphate. Thus, the band at 533 eV could be attributed not only to SiO$_2$, but also to P-OH and M-O-P species [70,73,79,80].

Contrary to Zr 3d core level, the binding energy of the photoelectronic Nb 3$d_{5/2}$ peak (207.6-207.9 eV) is almost unaltered with the phosphorus loading, and these values are in the typical range of Nb(V)

parameters declined more pronounced when the *ZrNbP0.2* catalyst suffers two calcination stages instead of one (*ZrNbP0.2-1c*). Therefore, it can be stated that synthetic methodology considerably affects the textural properties of catalysts. With regard to average pore diameters, all

in an oxidic environment [4,81], thus ruling out the presence of $NbOPO_4$ phases on the catalyst surface [82,83], as well as the interaction between niobium and phosphorus, corroborating NMR results.

Finally, the BE values for P 2*p* core level (133.2-134.5 eV) are characteristic of tetrahedral phosphorus [79,84,85] in phosphates. The width of bands makes difficult to assign the BE to an unique type of phosphate (such as PO_4^{3-}, HPO_4^{2-} or $H_2PO_4^{-}$) although the progressive shift of the band towards higher BE (Fig. S4) would indicate an increase of the P–O polarity, which can be enhanced by hydroxyls groups bonded to the phosphorus atoms [59,70,73]. Thus, the catalysts with higher Nb/P molar ratio display PO_4^{3-} species, which are progressively transformed into HPO_4^{2-} or $H_2PO_4^{-}$ as the molar ratio decreases, thus raising the amount of hydroxyl groups and hence the acidity of the catalysts.

Therefore, from XPS results, it can be concluded that the shifts observed in the Zr 3*d*, O 1*s* and P 2*p* spectra point to an increase of the amount of acid sites (POH groups) on the surface at higher P loadings.

The XPS analysis also provides useful information about the distribution of the different atoms on the surface of the catalysts. As it was inferred from the NMR analysis, phosphorus does not react with silica to form silicophosphates; moreover, from XPS analysis, it has been deduced that Zr shows a higher ionic character in the presence of phosphorus, and Nb is not affected by the presence of phosphorus. Therefore, it could be thought that zirconium and phosphorus interact when the latter is incorporated to catalysts, probably forming zirconium hydrogenphosphate. This phase is formed from the extracted zirconium of the silica network and it could explain why the Zr/(Si + Nb) atomic ratio rises with respect to the *ZrNb* catalyst when phosphorus is present (Table 2). These data are in accordance to XRD, textural and TEM analyses, where a partial destruction of the mesoporous structure occurs by incorporating P to the catalyst formulation. As it is shown in Table 2, the Nb/(Si + Zr) atomic ratio goes by a maximum for ZrNbP0.6 catalyst and in any case, this atomic ratio is superior to the ZrNb catalyst so it could be said that, as confirmed by the NMR analysis, the niobium is hardly interacting with P.

It is well known that activity in glycerol dehydration depends on the catalyst acidity. Although zirconium doped mesoporous silica, due to its acid character, has demonstrated to be active in this reaction [47], the niobium incorporation to the support (*ZrNb*) enhances the total acidity and acid strength as deduced from its NH_3-TPD profile (Table 1 and Fig. 5). Moreover, the strength of acid sites increases with the niobium loading, since the desorption peak at low temperature is shifted to higher values. Catalysts with a Nb/P molar ratio lower than 0.6 show a reduction of the acid sites concentration compared to the ZrNb catalyst. This means that the phosphorus must be interacting with acid sites of ZrNb catalyst, but without increasing the total amount of the acid sites. The formation of the hydrogenphosphate phase, as the Nb/P molar ratio is decreased, should be responsible of the noticeable increase of the acid sites above all for ZrNbP0.2-1c catalyst. NMR and XPS results suggested the formation of POH groups mainly bonded to Zr atoms, as far as phosphorus is incorporated. In the case of ZrNbP0.1 catalyst, a drastic reduction can be noted, being due to its textural properties are severely damaged. Thus, by normalizing the TPD data by the surface area (data in parentheses), the amount of NH_3 desorbed per square meter sharply increases with the P loading.

The catalyst with a Nb/P molar ratio of 0.2 shows the highest total acidity, especially when the calcination of precursors is carried out in a single step (*ZrNbP0.2-1c*), reaching an acidity value of 1010 μmoles $NH_3g_{cat}^{-1}$. Hence, the influence of calcination steps on acidity seems to be related to textural properties, since it has been demonstrated that the partial destruction of mesostructure is more drastic when the catalyst is subjected to two calcination processes at 400 °C. This increment of acidity has been previously observed by other authors for catalysts based on Nb_2O_5 after treatment with H_3PO_4 [43,45]. In the case of *ZrNbP0.1*, the catalyst with the highest P content, a drastic reduction can be noted, being due to its textural properties are severely damaged.
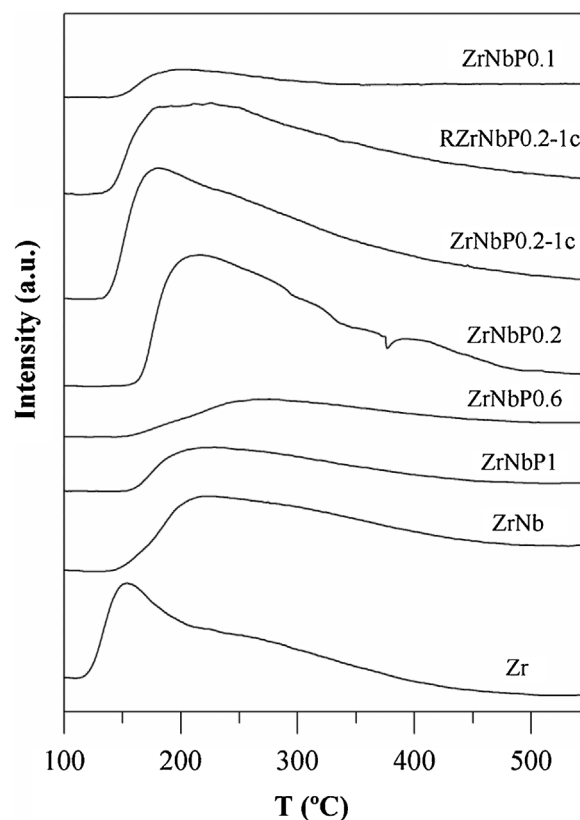

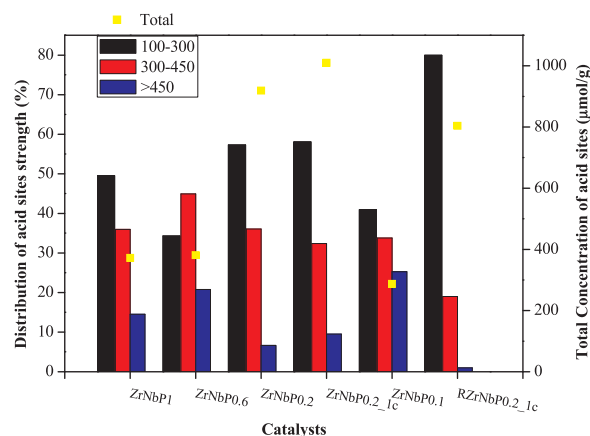**Fig. 5.** NH_3-TPD profiles of ZrNbP*x* catalysts.

Fig. 6. Histogram of proportion of acid sites as a function of desorption temperature for ZrNbP*x* catalysts.

Concerning the strength of acid sites, it depends on the phosphorus loading (Fig. 6). In general, the proportion of weak acid sites is predominant in comparison with medium and strong acid sites, except for the *ZrNbP0.6* catalyst, which shows a higher proportion of medium acid sites. The highest fraction of weak acid sites, along with the lowest of strong acid sites, is found for the *ZrNbP0.2* catalyst. This distribution of acid strength is related to the nature of superficial species; thus, although there are not experimental evidence supporting this assumption, it may be noted that the *ZrNbP0.6* catalyst showed the highest amount of superficial niobium, as was deduced from XPS analysis (Table 2). Therefore, niobium species could be responsible of the medium-strong acid sites. Recently, the influence of niobium species on the acid properties of niobium supported catalysts was reported, showing that the strength of acid sites increased as the loading of niobium was risen [49]. Furthermore, it should be pointed out that

catalysts containing zirconium hydrogenphosphate species have a more noticeable weak acid character.

On the other hand, the nature of acid sites is a key factor in determining the selectivity in glycerol dehydration. Pyridine adsorption coupled to FTIR spectroscopy is a well-known technique to evaluate the concentration of both Lewis and Brönsted acid sites. The FTIR spectra of catalysts after pyridine adsorption, after outgassing at 200 °C, (Fig. S5 and Table S3) display typical absorption bands associated to pyridine on Lewis (LAS) and Brönsted (BAS) acid sites [50,86]. Thus, *Zr* and *ZrNb* catalysts exhibit the presence of both types of acid sites (Table S3). As expected, the impregnation with phosphoric acid exerts a great influence on the nature and concentration of acid sites. Thus, the catalyst with the lowest phosphorus content (*ZrNbP1*) shows a significant decrease in Brönsted acid sites compared to the *ZrNb* catalyst. Likewise, the Lewis acid sites remain unaltered. These two findings might point out that the reaction of phosphoric acid has been taking place with surface OH groups, leaving the Lewis acid sites unreacted therefore these acid sites could be ascribed both to superficial niobium species and uncovered Zr(IV). Besides, the NH_3-TPD results showed that the total acidity of *ZrNbP1* was lower than that of *ZrNb*, in accordance with the pyridine results.

When the Nb/P molar ratio is further decreased to 0.6, the amount of both Brönsted and Lewis acid sites is increased. The generation of new Brönsted acid sites could be attributed to the zirconium hydrogenphosphate phase, already detected by NMR analysis (Fig. 2A). On the other hand, a higher amount of superficial niobium species, as demonstrated by XPS, would justify the increase of Lewis acidity.

The maximum concentration of Brönsted acid sites is reached for a Nb/P molar ratio of 0.2, which is even higher when the catalyst was undergone to one calcination step at 400 °C. This behavior is closely linked to the formation of zirconium hydrogenphosphate, whose P-OH groups possess a Brönsted acid character. On the other hand, the Lewis acidity is drastically reduced, indicating that the zirconium hydrogenphosphate must be covering the niobium species, associated to Lewis acid centers. These findings point out that the treatment with phosphoric acid favors the formation of new BAS, in such a way that the B/B + L ratio increases, even provoking the disappearance of LAS for a Nb/P molar ratio of 0.2 (Table S3). It has been previously reported that the treatment with phosphoric acid enhances the number of BAS [44,69], in agreement with the results obtained for *ZrNbP* catalysts. This fact is corroborated from their respective spectra, since the intensity of bands associated to BAS rises with respect to the support and Nb-based catalyst, disappearing the bands related to LAS (Fig. S6).

3.2. Catalytic results

These acid solid catalysts have been tested in glycerol dehydration at 325 °C, at atmospheric pressure. Acrolein, acetaldehyde and hydroxyacetone have been the detected products, whereas the rest of products not detected were grouping under the label "*others*". These "*others*" products could comprise compounds such as allyl alcohol, propanaldehyde, acetone, ethanol etc...but those compounds have been not detected by the analytical procedure (GC-FID, see Experimental section) probably because they concentration is lower than the detection limit of the technique.

The catalytic performance of both *Zr* and *ZrNb* catalysts has been reported in a previous paper [49], henceforth, their catalytic results will be presented if it is necessary for comparison reasons; in any case, their main catalytic data are also compiled in Table 3.

The catalytic behaviour reflects the influence of the phosphorus loading (Table 3), in such a way that catalysts with a Nb/P molar ratio of 0.6 and 1 show, after 2 h of TOS, a glycerol conversion even lower than that of the *ZrNb* catalyst (Table 3). However, for lower Nb/P molar ratio, the conversion increases considerably up to reaching complete glycerol conversion with the *ZrNbP0.2-1c* catalyst. On the other hand, it is interesting to highlight that the catalysts without zirconium (*NbP0.2-*

Table 3
Glycerol conversion and product selectivities over studied catalysts.

Sample	C_{Gly} (%)	S_{Acrol} (%)	S_{Actal} (%)	S_{HyA} (%)	S_{Others} (%)	C (%)
Zr	91 (72)	25 (23)	22 (20)	5 (7)	49 (50)	55 (64)
ZrNb	80 (51)	36 (34)	11 (9)	8 (6)	45 (51)	64 (74)
ZrNbP1	67 (49)	38 (35)	6 (5)	6 (4)	50 (56)	66 (73)
ZrNbP0.6	69 (44)	37 (42)	4 (4)	3 (5)	56 (49)	61 (78)
ZrNbP0.2	84 (61)	51 (43)	0 (0)	9 (7)	41 (49)	66 (70)
ZrNbP0.2-1c	100 (85)	56 (44)	0 (0)	10 (11)	34 (35)	66 (70)
ZrNbP0.1	74 (53)	53 (49)	0 (0)	8 (6)	39 (46)	71 (76)
ZrP0.2-1c	89 (62)	37 (23)	0.2 (0.2)	10 (4)	53 (73)	53 (55)
NbP0.2-1c	76 (42)	34 (35)	0.2 (0.3)	2 (0.4)	64 (65)	51 (73)
ZrHPO₄	4 (7)	66 (16)	0 (0)	0 (0)	34 (84)	98 (94)
NbOPO₄	37 (14)	36 (60)	3 (8)	0 (0)	61 (32)	77 (95)

Data measured after 2 h and 8 h (in parentheses); Gly = glycerol; Acrol = acrolein; Actal = acetaldehyde; HyA = hydroxyacetone. C (%) = carbon balance
Experimental conditions: weight of catalyst = 0.5 g diluted with SiC to 3 cm^3 volume. Feed composition: 10 wt% glycerol in water; liquid flow = 0.1 mL min^{-1}; N_2 flow = 15 mL min^{-1}. T = 325 °C.

1c), or niobium (*ZrP0.2-1c*), are also very active, but less selective to acrolein, indicating that both niobium and zirconium species are involved in the catalytic process, but with a different selectivity pattern.

As regards the catalyst stability, all catalysts suffer a gradual deactivation as the reaction proceeds, and after 8 h of reaction, the decrease of glycerol conversion is between 15 and 25% of the initial values. However, there is not a clear trend based on the phosphorus loading. The highest stability is attained by using the catalyst prepared with one calcination step. The low carbon balance values and the black color of used catalysts also corroborate that deactivation is taking place.

3.2.1. Influence of density of acid sites

In general, the glycerol conversion increases with the concentration of acid sites (Fig. 7). When the Nb/P molar ratio is lowered from 1 to 0.6, the conversion slightly enhances since both catalysts display quite similar acid and textural properties, and consequently a significant improvement of the activity is not achieved. However, the *ZrNbP0.1* catalyst falls out of this trend, and its catalytic activity is higher than those of catalysts with a higher Nb/P molar ratio in spite of its lower acid site concentration. However, it is noteworthy that this catalyst possesses both the lowest total acidity and specific surface area (Fig. S6), which lead to the highest density of acid centers (*ca.* 6 acid sites nm^{-2}), thereby increasing the glycerol conversion in comparison with the *ZrNbP1* and *ZrNbP0.6* catalysts. But, on the other hand, a high density of acid sites could imply that not all acid sites can be simultaneously available for glycerol molecules, because steric hindrances should be taken into consideration. They may arise between glycerol
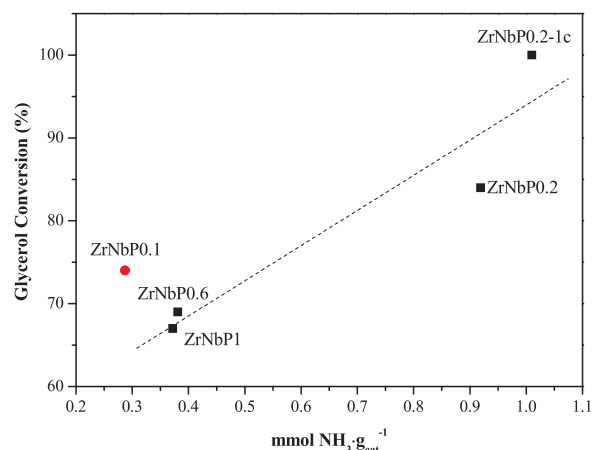

Fig. 7. Glycerol conversion as function of the acidity of ZrNbP*x* catalysts expressed as mmol $NH_3 \cdot g_{cat}^{-1}$.

molecules close enough hindering their reaction [87], which renders the *ZrNbP0.1* catalyst less active than the *ZrNbP0.2* catalyst. Therefore, both high density of acid sites and its availability plays an important role to be active catalyst [88–90].

The increased density of acid sites with the phosphorus loading is related to the formation of zirconium hydrogenphosphate. Although this phase does not present a high crystallinity and knowing that the distance between two adjacent hydroxyl acid groups for zirconium hydrogenphosphate is only 0.53 nm [88], and considering that the cross section of glycerol is 0.3 nm^2 [87], it can be assumed that a high fraction of these acid sites will not be available for reaction at the same time.

According to the present results, the highest glycerol conversion was achieved with the catalyst having c.a. 2 acid sites nm^{-2}, which corresponds to the *ZrNbP0.2-1c* catalyst. This catalyst shows appropriate acid and textural properties to perform successfully the glycerol dehydration, since the porous structure is maintained after the acid treatment and, on the other hand, it presents the highest acid site concentration. Both properties provide an optimal distribution of acid sites for reaching a higher catalytic performance.

The influence of acid sites density on the catalytic performance can also be followed by plotting Turn Over Frequency (TOF) values at time zero versus this density (Fig. 8) to avoid the negative influence of the deactivation on the catalytic performance. This measurement has been carried out following the assumption proposed by Choi et al. [87], who assume an exponential catalyst deactivation with Time On Stream (TOS). This Figure shows that catalysts having the lowest density of acid sites display the highest TOF values, whereas an increase of density leads to drastic diminution of TOF values, except for the *ZrNbP0.1* catalyst. In this case, the high TOF value could be ascribed to both the availability of acid sites and lower mass transfer limitations, because this catalyst possesses large pore sizes, in the range of macropores (Fig. 4).

3.2.2. Influence of nature of acid sites on the reaction selectivity

The selectivity will depend on the nature of acid sites, that is, their Brönsted or Lewis character. In general, it is largely accepted that Brönsted acid sites are involved in the formation of acrolein, and the Lewis acidity favor hydroxyacetone (acetol) [36,37,48]. The influence of Brönsted acid sites on the acrolein yield is proved in Fig. 9, where the acrolein yield increases as the Brönsted acid sites does, except the *ZrNbP0.6* catalyst. This exhibits an acrolein yield similar to the *ZrNbP1* catalyst in spite of its higher concentration of Brönsted acid sites. However, if all active sites were accessible, the *ZrNbP0.6* catalyst would show an acrolein yield similar to that of *ZrNbP0.2*, and consequently another element must influence on its catalytic activity. Thus, the effect
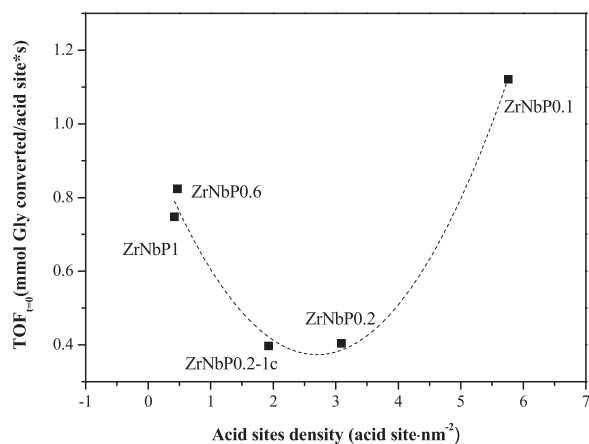

Fig. 9. Acrolein yield over ZrNbP*x* catalysts as a function of Brönsted acid sites concentration expressed as mmol·g$_{cat}$$^{-1}$ (0.5 g diluted with SiC to 3 cm^3 volume; 0.1 mL min^{-1} of 10 wt.% glycerol in water; N$_2$ flow = 15 mL min^{-1} and 325 °C).

Fig. 10. Influence of S$_{BET}$ on the rate of acrolein production per m^2.

of specific surface area on the production rate of acrolein per square meter was studied (Fig. 10), and similar values are obtained for catalysts having a Brönsted acidity quite dissimilar.

Moreover, it is noteworthy to mention the variation of hydroxyacetone selectivity as function of the Lewis acidity. It would be expected that catalysts with the highest concentration of Lewis acid sites should be the most selective towards hydroxyacetone, but an opposite trend is observed. In this sense, the catalyst with the lowest concentration of Lewis acid sites was the most selective towards hydroxyacetone. On the other hand, the acetaldehyde formation has been described in terms of retro-aldol reaction from unstable 3-hydroxypropanal intermediate [89,90], but also from hydroxyacetone [34,91,92]. According to the present catalytic results, the most selective catalysts to acetaldehyde are those whose selectivity to hydroxyacetone is lower and hence, likely, the acetaldehyde is evolved from hydroxyacetone. Consequently, the hydroxyacetone selectivity is lower in spite of their higher Lewis acid site concentration. The strength of acid sites is likely playing a key role in these secondary reactions, along with the nature of acid sites. Thus, the *ZrNbP1* and *ZrNbP0.6* catalysts display a higher proportion of medium–strong acid sites (> 50%) and they are the most selective to acetaldehyde, whereas the *ZrNbP0.2* and *ZrNbP0.2-1c* catalysts with a lower proportion are the most selective to hydroxyacetone, and acetaldehyde is not detected. Moreover, the acetaldehyde formation is detrimental to the acrolein selectivity since it has been described as an intermediate [34] for the formation of compounds like phenol from the reaction with acrolein. This fact could also be the cause of the lower selectivity shown by these catalysts (Table 3).

Fig. 8. Conversion rate of glycerol per acid site present in the catalysts at time zero (TOF$_{(t\,=\,0)}$) versus total concentration of acid sites per square nanometer.
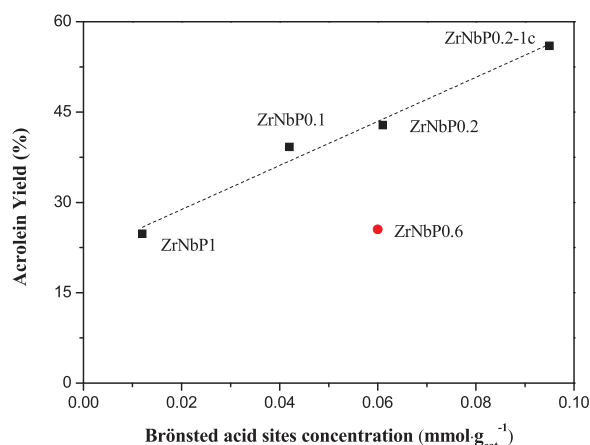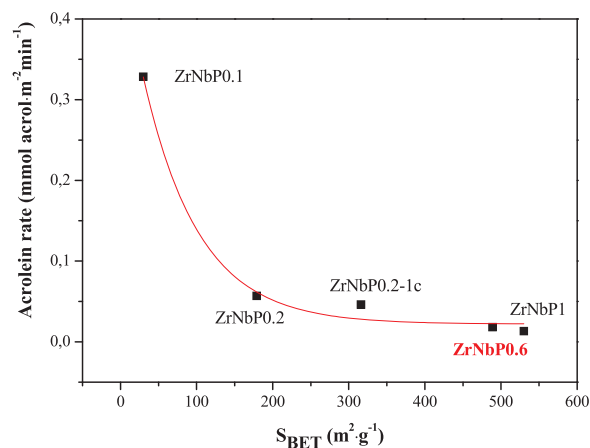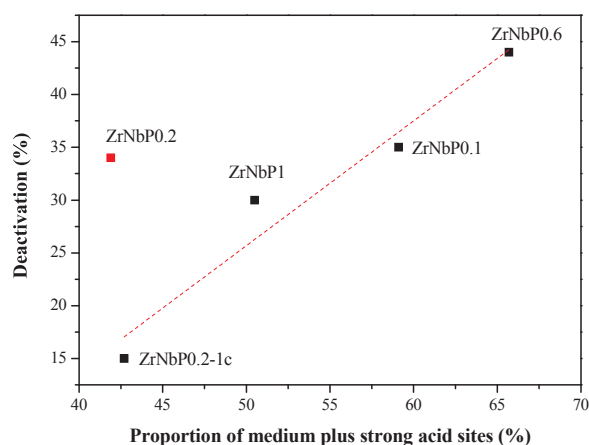
Fig. 11. Catalytic deactivation *vs* proportion of medium-strong acid sites.

3.2.3. Influence of acid strength on the catalysts stability

On the other hand, another parameter related to the catalytic activity is the strength of acid sites because such variable has been associated to the long-term catalyst stability [8,25,34,93], although other authors have proposed that strong acid sites are required for attaining a high acrolein yield [20,94]. The distribution of acid site strength could have an important impact on both the catalytic activity and stability. Thus, the catalysts with the lowest proportion of strong acid sites are more active and stable with TOS. Moreover, these catalysts also showed the highest proportion of Brönsted acid sites, therefore, it can be concluded that such Brönsted acid sites would be weak. This behavior is depicted in Fig. 11 where the catalyst deactivation is plotted versus the proportion of strong and medium acid sites. The catalyst deactivation was evaluated as the percentage of glycerol conversion depletion from t = 0 h to t = 8 h. This plot shows a linear relationship between catalyst deactivation and strength of acid sites. Thus, the catalyst with the highest proportion of strong acid sites exhibits the major deactivation. However, the *ZrNbP0.2* catalyst does not follow this trend. The acidity of this catalyst, measured as percentage of strength of acid sites, is quite similar to those of the *ZrNbP0.2-1c*, but the deactivation is more sharpened. Comparing the textural properties of both catalysts, the catalyst synthesized by using two calcination steps showed lower specific surface area along and pore volume. It seems clear that textural properties are also influencing over the catalyst deactivation.

In this context, the deactivation has been associated to the adsorption of high boiling point products on the catalyst surface, which can promote coke formation. This fact is proved by the black color of used catalysts and the low carbon balance (Table 3). The coke evolution is fully demonstrated by elemental analysis (Table S4), with carbon contents comprised between 5.2 and 5.9 wt%. The *ZrNbP0.1* catalyst exhibits the lowest value, but it is worthy to recall that this catalyst has the lowest S_{BET} and pore volume. These carbon contents, themselves, do not explain why some of the catalysts are deactivated more than others. The catalysts with the lowest phosphorus loading, after the catalytic process, showed a marked reduction of BET surface area (Table 1) in

spite of similar carbon contents detected in all catalysts. These catalysts should be able to spread the carbonaceous deposits in such way that the lowest reduction of the BET area took place. It could be expected that the coke formation was favored over the catalysts with the highest amount of strong acid sites [95,96], i.e. *ZrNbP1* and *ZrNbP0.6* catalysts, but this does not occur. It can be affirmed that deactivation is not only due to coke formation but also depends on the nature of acid sites, which will affect the nature of carbonaceous deposits. Thus, the most selective catalysts towards hydroxyacetone are the most stable ones. Moreover, those catalysts are characterized by B/B + L ratio close to one, i.e. they are basically Brönsted acid catalysts. Therefore, on those catalysts, it is likely that hydroxyacetone does not evolve to other products, like acetaldehyde [34], and the highest hydroxyacetone selectivity is achieved. Conversely, *ZrNbP1* and *ZrNbP0.6* catalysts with a lower B/B + L ratio, with a measurable concentration of Lewis acid sites (Table S3), should achieve the highest hydroxyacetone selectivity, but instead, the hydroxyacetone is converted into acetaldehyde. This latter process could be favored by the presence of Lewis acid sites. The presence of Lewis acidity could exert a double effect, on the one hand, to decrease the selectivity to hydroxyacetone because it is transformed into other reaction products, and, on the other hand, compounds arisen from hydroxyacetone can react with acrolein forming aromatic compounds like phenol, thus decreasing the selectivity to acrolein [34,92]. Therefore, it could be concluded that Lewis acid sites have a detrimental effect on the catalyst stability.

3.2.4. Influence of temperature of reaction

The most suitable catalytic performance of the *ZrNbP0.2-1c* catalyst encourages us to carry out a study above the influence of other experimental variables, like reaction temperature (Table 4). Both glycerol conversion and acrolein selectivity enhance when the reaction temperature increases from 300 °C up to 350 °C, reaching values of 100% and 74%, respectively, after 2 h on stream at 350 °C, and keeping 84% and 56% after 8 h of TOS, under these experimental conditions. This leads to a value of acrolein yield as high as 74%. at 350 °C.

On the other hand, acetaldehyde and hydroxyacetone yields stay almost unaltered in the studied range of temperatures, confirming that the formation of these products is only related to the nature of acid sites. Finally, the amount of not detected products decreases with the reaction temperature, according with data reported by Corma et al. [13].

3.2.5. Catalyst deactivation

Finally, the catalyst deactivation is an important drawback in glycerol dehydration to acrolein. It can be inferred from the decrease of glycerol conversion, from 100%, after 2 h of TOS, until 39%, after 24 h, with the *ZrNbP0.2-1c* catalyst at 350 °C, with a concomitant decrease of acrolein selectivity from 74% until 42% (Fig. 12). In order to deepen into the nature of adsorbed species over catalyst surface, the spent *ZrNbP0.2-1c* catalyst (denoted as *SZrNbP0.2-1c*) has been characterized. Firstly, the carbon content, as determined by CHN analysis, is 7.8% after 24 h on stream, which confirms the presence of carbonaceous deposits. The study by XPS indicates that the atomic concentrations of

Table 4

Glycerol conversion and product selectivities over ZrNbP0.2-1c at different reaction temperatures and regenerated ZrNbP0.2-1c.

Sample	T^a	C_{Gly} (%)	S_{Acrol} (%)	S_{Actal} (%)	S_{HyA} (%)	S_{Others} (%)	C (%)
ZrNbP0.2-1c	300	88 (62)	55 (54)	0 (0)	11 (11)	34 (34)	70 (79)
ZrNbP0.2-1c	325	100 (85)	56 (44)	0 (0)	10 (11)	34 (35)	66 (70)
ZrNbP0.2-1c	350	100 (84)	74 (56)	0.2 (0.7)	8 (15)	17 (26)	82 (78)
*RZrNbP0.2-1c	350	99 (87)	73 (37)	1 (1)	4 (9)	22 (53)	79 (54)

Data measured after 2 h and 8 h (in brackets); Gly = glycerol; Acrol = acrolein; Actal = acetaldehyde; HyA = hydroxyacetone. C (%) = carbon balance
Experimental conditions: weight of catalyst = 0.5 g diluted with SiC to 3 cm^3 volume. Feed composition: 10 wt% glycerol in water; liquid flow = 0.1 mL min^{-1}; N$_2$ flow = 15 mL min^{-1}.
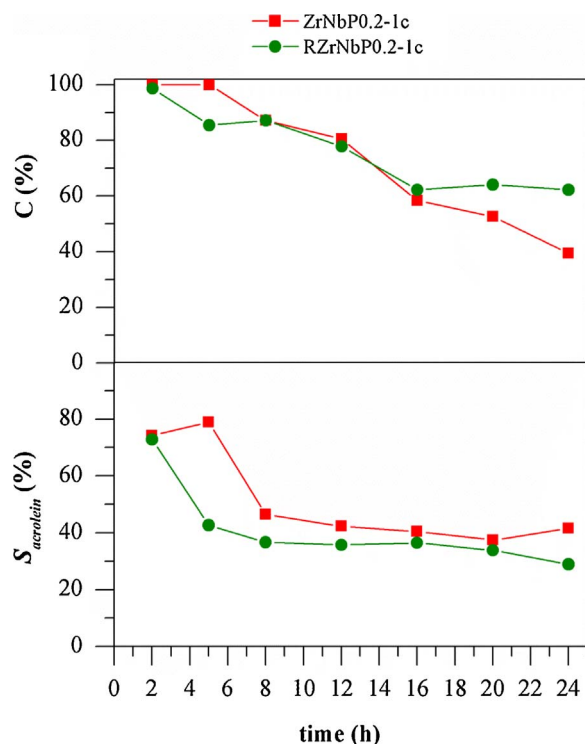* RZrNbP0.2-1c regenerated.

Fig. 12. Influence of regeneration treatment on glycerol conversion and acrolein selectivity over ZrNbP0.2-1c catalyst as a function of the reaction time (0.5 g diluted with SiC to 3 cm^3 volume; 0.1 mL min^{-1} of 10 wt.% glycerol in water and N$_2$ flow = 15 mL min^{-1} and 350 °C).

structural elements are unchanged (Table S5), in spite of the high percentage of carbon on the catalyst surface.

Therefore, the regeneration of spent catalyst has been accomplished by thermal treatment at 550 °C for 4 h, under an air flow (15 mL min^{-1}), considering the thermal stability of carbonaceous deposits inferred from DTA-TG curves (not shown). The regenerated catalyst, *RZrNbP0.2-1c*, has been reused under similar experimental conditions (350 °C and 24 h of TOS). According to the activity data, a similar trend is attained for glycerol conversion during the first 16 h of TOS with respect to fresh catalyst, and it can be observed that the deactivation is lower for regenerated catalyst, maintaining a glycerol conversion of 62.2% after 24 h. This fact may be explained by a lowering of total acidity, as a consequence of the thermal treatment, which minimizes the catalyst deactivation. However, this reduction of total acidity influences negatively on acrolein selectivity, in such a way that lower values are achieved for regenerated catalyst after 5 h of TOS (Fig. 12). This reduction may be also related to the slight modification of acid properties of *ZrNbP0.2-1c* during the regeneration treatment, in such a way that the total acidity decrease from 1010 up to 804 μmoles NH$_3$ g$_{cat}$$^{-1}$ and the B/B + L ratio diminishes from 1.00 until 0.96. Therefore, a lower amount of Brönsted acid sites can provoke that acrolein selectivity decreases, since it has been demonstrated before that BAS are more selective to acrolein than LAS. In any case, these differences are almost negligible, since both glycerol conversion and acrolein selectivity for *RZrNbP0.2-1c* follow a similar trend than the fresh catalyst (Fig. 12). Moreover, the stability of active phases has been demonstrated by XPS, because the atomic concentrations of Nb, Zr and P are maintained after the regeneration treatment (Table S5). Lee et al. [45] attributed the deactivation of PO$_4$/Nb$_2$O$_5$ catalyst to the leaching of phosphorus species during the catalytic run, but in our case this fact did not take place and such observed deactivation was due to the formation of carbonaceous deposits on active sites. Therefore, it has been proven that this catalyst can be reused under these experimental conditions, recovering its activity by thermal treatment (Fig. 12 and Table 3).

4. Conclusions

A catalyst with a 8 wt% Nb$_2$O$_5$ supported on a zirconium doped mesoporous silica has been treated with different amounts of phosphoric acid (Nb/P = 0.1-1), modifying their textural and acid properties. The phosphorus incorporation damages the textural properties and modifies the nature of acid sites, increasing the B/B + L ratio. Likewise, the synthesis methodology influences on the textural properties, since the deterioration of silica mesostructure is less pronounced when the calcination of precursors is carried out in a single stage. It has been demonstrated that glycerol conversion increases with the P content, which is explained by the formation of zirconium hydrogenphosphate. Thus, the catalyst with a Nb/P = 0.2 calcined in a step (*ZrNbP0.2-1c*) possesses the most suitable distribution of acid sites, which together with a less damaged structure and the highest acid sites concentration, allows achieving a total glycerol conversion and an acrolein yield of 74% after 2 h of time on stream, at 350 °C. Moreover, although it deactivates after 24 h of TOS, the catalyst can be regenerated by thermal treatment at 550 °C for 4 h in air flow, recovering its catalytic activity.

Appendix A. Supplementary data

Supplementary data associated with this article can be found, in the online version, at http://dx.doi.org/10.1016/j.apcatb.2017.09.016.

References

[1] L. Meher, D. Sagar, S. Naik, Renew. Sustain. Energy Rev. 10 (2006) 248–268.
[2] J. Almeida, L. Favaro, B. Quirino, Biotechnol. Biofuels 5 (2012).
[3] E. Shahid, Y. Jamal, Renew. Sustain. Energy Rev. 15 (2011) 4732–4745.
[4] M. Massa, A. Andersson, E. Finocchio, G. Busca, J. Catal. 307 (2013) 170–184.
[5] C.A.G. Quispe, C.J.R. Coronado, J.A. Carvalho Jr., Renew. Sustain. Energy Rev. 27 (2013) 475–493.
[6] L. Liu, X. Ye, J. Bozell, ChemSusChem 5 (2012) 1162–1180.
[7] B. Katryniok, S. Paul, M. Capron, F. Dumeignil, ChemSusChem 2 (2009) 719–730.
[8] L. Shen, Y. Feng, H. Yin, A. Wang, L. Yu, T. Jiang, Y. Shen, Z. Wu, J. Ind. Eng. Chem. 17 (2011) 484–492.
[9] E. Kraleva, R. Palcheva, L. Dimitrov, U. Armbruster, A. Bruckner, A. Spojakina, J. Mater. Sci. 46 (2011) 7160–7168.
[10] Y.T. Kim, K.D. Jung, E.D. Park, B. Korean Chem. Soc. 31 (2010) 3283–3290.
[11] B. Katryniok, S. Paul, M. Capron, C. Lancelot, V. Belliere-Baca, P. Rey, F. Dumeignil, Green Chem. 12 (2010) 1922–1925.
[12] R. Liu, T. Wang, Y. Jin, Catal. Today 233 (2014) 127–132.
[13] A. Corma, G. Huber, L. Sauvanauda, P. O'Connor, J. Catal. 257 (2008) 163–171.
[14] Y. Kim, K. Jung, E. Park, Micropor. Mesopor. Mater. 131 (2010) 28–36.
[15] C. Jia, Y. Liu, W. Schmidt, A. Lu, F. Schuth, J. Catal. 269 (2010) 71–79.
[16] A. de Oliveira, S. Vasconcelos, J. de Sousa, F. de Sousa, J. Filho, A. Oliveira, Chem. Eng. J. 168 (2011) 765–774.
[17] A. Ulgen, W. Hoelderich, Catal. Lett. 131 (2009) 122–128.
[18] S. Vasconcelos, C. Lima, J. Mendes, A. Oliveira, E. Barros, F. de Sousa, M. Rocha, P. Bargiela, Chem. Eng. J. 168 (2011) 656–664.
[19] N. Shiju, D. Brown, K. Wilson, G. Rothenberg, Top. Catal. 53 (2010) 1217–1223.
[20] L. Tao, B. Yan, Y. Liang, B. Xu, Green Chem. 15 (2013) 696–705.
[21] W. Suprun, M. Lutecki, T. Haber, H. Papp, J. Mol. Catal. A: Chem. 309 (2009) 71–78.
[22] F. Wang, J. Dubois, W. Ueda, J. Catal. 268 (2009) 260–267.
[23] F. Wang, J. Dubois, W. Ueda, Appl. Catal. A: Gen. 376 (2010) 25–32.
[24] Q. Liu, Z. Zhang, Y. Du, J. Li, X. Yang, Catal. Lett. 127 (2009) 419–428.
[25] F. Cavani, S. Guidetti, L. Marinelli, M. Piccinini, E. Ghedini, M. Signoretto, Appl. Catal. B: Environ. 100 (2010) 197–204.

[26] L. Yang, J. Joo, N. Kim, K. Jung, J. Yi, Korean J. Chem. Eng. 27 (2010) 1695–1699.
[27] J. Lourenco, M. Macedo, A. Fernandes, Catal. Commun. 19 (2012) 105–109.
[28] K. Pathak, K. Reddy, N. Bakhshi, A. Dalai, Appl. Catal. A: Gen. 372 (2010) 224–238.
[29] K. Nakajima, Y. Baba, R. Noma, M. Kitano, J. Kondo, S. Hayashi, M. Hara, J. Am. Chem. Soc. 133 (2011) 4224–4227.
[30] I. Nowak, M. Ziolek, Chem. Rev. 99 (1999) 3603–3624.
[31] S. Chai, H. Wang, Y. Liang, B. Xu, J. Catal. 250 (2007) 342–349.
[32] K. Omata, S. Izumi, T. Murayama, W. Ueda, Catal. Today 201 (2013) 7–11.
[33] P. Lauriol-Garbay, J. Millet, S. Loridant, V. Belliere-Baca, P. Rey, J. Catal. 280 (2011) 68–76.
[34] P. Lauriol-Garbey, G. Postole, S. Loridant, A. Auroux, V. Belliere-Baca, P. Rey, J. Millet, Appl. Catal. B: Environ. 106 (2011) 94–102.
[35] M. Massa, A. Andersson, E. Finocchio, G. Busca, F. Lenrick, L. Wallenberg, J. Catal. 297 (2013) 93–109.
[36] A. Alhanash, E. Kozhevnikova, I. Kozhevnikov, Appl. Catal. A: Gen. 378 (2010) 11–18.
[37] B. Katryniok, S. Paul, F. Dumeignil, ACS Catal. 3 (2013) 1819–1834.
[38] S. Chai, H. Wang, Y. Liang, B. Xu, Green Chem. 9 (2007) 1130–1136.
[39] J. Jehng, I. Wachs, E. Ko, Catal. Today 8 (1990) 37–55.
[40] M. Shirai, N. Ichikuni, K. Asakura, Y. Iwasawa, Catal. Today 8 (1990) 57–66.
[41] S. Okazaki, A. Kurosaki, Catal. Today 8 (1990) 113–122.
[42] S. Okazaki, M. Kurimata, T. Iizuka, K. Tanabe, B. Chem. Soc. Jpn. 60 (1987) 37–41.
[43] Z. Tang, D. Yu, P. Sun, H. Li, H. Huang, B. Korean Chem. Soc. 31 (2010) 3679–3683.
[44] J. Ekhsan, S. Lee, H. Nur, Appl. Catal. A: Gen. 471 (2014) 142–148.
[45] Y.Y. Lee, K.A. Lee, N.C. Park, Y.C. Kim, Catal. Today 232 (2014) 114–118.
[46] Y. Choi, D. Park, H. Yun, J. Baek, D. Yun, J. Yi, ChemSuschem 5 (2012) 2460–2468.
[47] C. Garcia-Sancho, R. Moreno-Tost, J. Merida-Robles, J. Santamaria-Gonzalez, A. Jimenez-Lopez, P. Maireles-Torres, Appl. Catal. A: Gen. 433 (2012) 179–187.
[48] B. Katryniok, S. Paul, V. Belliere-Baca, P. Rey, F. Dumeignil, Green Chem. 12 (2010) 2079–2098.
[49] C. García-Sancho, J.A. Cecilia, A. Moreno-Ruiz, J.M. Mérida-Robles, J. Santamaría-González, R. Moreno-Tost, P. Maireles-Torres, Appl. Catal. B: Environ. 179 (2015) 139–149.
[50] J. Datka, A. Turek, J. Jehng, I. Wachs, J. Catal. 135 (1992) 186–199.
[51] J. Sun, H. Zhang, D. Ma, Y. Chen, X. Bao, A. Klein-Hoffmann, N. Pfander, D. Su, Chem. Commun. (2005) 5343–5345.
[52] B. Wu, Z. Tong, X. Yuan, J. Porous Mater. 19 (2012) 641–647.
[53] P. Colomban, A. Novak, J. Mol. Struct. 198 (1989) 277–295.
[54] Y. Huang, Q. Li, T. Anfimova, E. Christensen, M. Yin, J. Jensen, N. Bjerrum, W. Xing, Int. J. Hydrogen Energy 38 (2013) 2464–2470.
[55] S. Pavlova, V. Sadykov, G. Zabolotnaya, D. Kochubey, R. Maximovskaya, V. Zaikovskii, V. Kriventsov, S. Tsybulya, E. Burgina, A. Volodin, M. Chaikina, N. Kuznetsova, V. Lunin, D. Agrawal, R. Roy, J. Mol. Catal. A: Chem. 158 (2000) 319–323.
[56] W. Liu, Z. Song, T. Ikegawa, H. Nishiguchi, T. Ishihara, Y. Takita, Mater. Lett. 58 (2004) 3328–3331.
[57] J. Jimenez-Jimenez, P. Maireles-Torres, P. Olivera-Pastor, E. Rodriguez-Castellon, A. Jimenez-Lopez, D. Jones, J. Roziere, Adv. Mater. 10 (1998) 812–815.
[58] H. Benhamza, P. Barboux, A. Bouhaouss, F. Josien, J. Livage, J. Mater. Chem. 1 (1991) 681–684.
[59] R. Weingarten, Y. Kim, G. Tompsett, A. Fernandez, K. Han, E. Hagaman, W. Conner, J. Dumesic, G. Huber, J. Catal. 304 (2013) 123–134.
[60] K. Segawa, Y. Nakajima, S. Nakata, S. Asaoka, H. Takahashi, J. Catal. 101 (1986) 81–89.
[61] A. Alfaya, Y. Gushikem, S. de Castro, Micropor. Mesopor. Mater. 39 (2000) 57–65.
[62] M. Francisco, W. Cardoso, Y. Gushikem, R. Landers, Y. Kholin, Langmuir 20 (2004) 8707–8714.

[63] N. Clayden, S. Esposito, P. Pernice, A. Aronne, J. Mater. Chem. 11 (2001) 936–943.
[64] T. Krawietz, P. Lin, K. Lotterhos, P. Torres, D. Barich, A. Clearfield, J. Haw, J. Am. Chem. Soc. 120 (1998) 8502–8511.
[65] N.J. Clayden, G. Accardo, P. Mazzei, A. Piccolo, P. Pernice, A. Vergara, C. Ferone, A. Aronne, J. Mater. Chem. A 3 (2015) 15986–15995.
[66] D. Spielbauer, G. Mekhemer, T. Riemer, M. Zaki, H. Knozinger, J. Phys. Chem. B 101 (1997) 4681–4688.
[67] P. Armento, M. Casciola, M. Pica, F. Marmottini, R. Palombari, F. Ziarelli, Solid State Ionics 166 (2004) 19–25.
[68] K. Kao, C. Mou, Micropor. Mesopor. Mater. 169 (2013) 7–15.
[69] J.A. Cecilia, C. García-Sancho, J.M. Mérida-Robles, J. Santamaría-González, R. Moreno-Tost, P. Maireles-Torres, Catal. Today 254 (2015) 43–52.
[70] G. Alberti, U. Costantino, G. Marletta, O. Puglisi, S. Pignataro, J. Inorg. Nucl. Chem. 43 (1981) 3329–3334.
[71] H. Bosman, A. Pijpers, A. Jaspers, J. Catal. 161 (1996) 551–559.
[72] S. Damyanova, P. Grange, B. Delmon, J. Catal. 168 (1997) 421–430.
[73] J. Colon, D. Thakur, C. Yang, A. ClearfieldL, C. Martin, J. Catal. 124 (1990) 148–159.
[74] E. Farfan-Torres, E. Sham, M. Martínez-Lara, A. Jiménez-López, Mater. Res. Bull. 27 (1992) 1255–1262.
[75] E. Rodriguez-Castellon, A. Jimenez-Lopez, P. Maireles-Torres, D. Jones, J. Roziere, M. Trombetta, G. Busca, M. Lenarda, L. Storaro, J. Solid. State. Chem. 175 (2003) 159–169.
[76] B. Chowdari, K. Tan, W. Chia, R. Gopalakrishnan, J. Non Cryst. Solids 119 (1990) 95–102.
[77] G. Khattak, M. Salim, A. AlHarthi, D. Thompson, L. Wenger, J. Non Cryst. Solids 212 (1997) 180–191.
[78] L. Lisi, G. Ruoppolo, M. Casaletto, P. Galli, M. Massucci, P. Patrono, F. Pinzari, J. Mol. Catal. A: Chem. 232 (2005) 127–134.
[79] Z. Yuan, T. Ren, A. Azioune, J. Pireaux, B. Su, Catal. Today 105 (2005) 647–654.
[80] A. Majjane, A. Chahine, M. Et-tabirou, B. Echchahed, T. Do, P. Mc Breen, Mater. Chem. Phys. 143 (2014) 779–787.
[81] J. Yan, G. Wu, N. Guan, L. Li, Appl. Catal. B: Environ. 152–153 (2014) 280–288.
[82] P. Pereira, H. Voorwald, M. Cioffi, M. Da Silva, A. Rego, A. Ferraria, M. De Pinho, Cellulose 21 (2014) 641–652.
[83] M. de Pietre, L. Almeida, R. Landers, R. Vinhas, F. Luna, React. Kinet. Mech. Catal. 99 (2010) 269–280.
[84] A. Puziy, O. Poddubnaya, A. Ziatdinov, Appl. Surf. Sci. 252 (2006) 8036–8038.
[85] X. Fan, T. Yu, Y. Wang, J. Zheng, L. Gao, Z. Li, J. Ye, Z. Zou, Appl. Surf. Sci. 254 (2008) 5191–5198.
[86] G. Busca, Catal. Today 41 (1998) 191–206.
[87] Y. Choi, H. Park, Y. Yun, J. Yi, ChemSusChem 8 (2015) 974–979.
[88] R. Slade, J. Knowles, D. Jones, J. Roziere, Solid State Ionics 96 (1997) 9–19.
[89] S. Lopez-Pedrajas, R. Estevez, R. Navarro, D. Luna, F. Bautista, J. Mol. Catal. A: Chem. 421 (2016) 92–101.
[90] M. Dalil, D. Carnevali, M. Edake, A. Auroux, J. Dubois, G. Patience, J. Mol. Catal. A: Chem. 421 (2016) 146–155.
[91] R. Liu, T. Wang, D. Cai, Y. Jin, Ind. Eng. Chem. Res. 53 (2014) 8667–8674.
[92] P. Lauriol-Garbey, J. Millet, S. Loridant, V. Belliere-Baca, P. Rey, J. Catal. 281 (2011) 362–370.
[93] W. Suprun, M. Lutecki, R. Glaser, H. Papp, J. Mol. Catal. A: Chem. 342–43 (2011) 91–100.
[94] B. Dalla Costa, M. Peralta, C. Querini, Appl. Catal. A: Gen. 472 (2014) 53–63.
[95] Y. Gu, N. Cui, Q. Yu, C. Li, Q. Cui, Appl. Catal. A: Gen. 429 (2012) 9–16.
[96] C. Carrico, F. Cruz, M. Santos, H. Pastore, H. Andrade, A. Mascarenhas, Micropor. Mesopor. Mater. 181 (2013) 74–82.